IEEE Access
Multidisciplinary | Rapid Review | Open Access Journal

Received September 11, 2020, accepted September 23, 2020, date of publication September 28, 2020,
date of current version October 8, 2020.

Digital Object Identifier 10.1109/ACCESS.2020.3027478

Mechanical Fault Diagnosis of High Voltage Circuit Breakers Utilizing VMD Based on Improved Time Segment Energy Entropy and a New Hybrid Classifier

CHENGCHENG CAO[1], MINGLIANG LIU[1,2], BING LI[1], AND YUNXIA WANG[1,2]
[1]HLJ Province Key Laboratory of Senior-Education for Electronic Engineering, Heilongjiang University, Harbin 150080, China
[2]Key Laboratory of Information Fusion Estimation and Detection, Heilongjiang Province, Harbin 150080, China

Corresponding authors: Mingliang Liu (2002039@hlju.edu.cn) and Yunxia Wang (2001019@hlju.edu.cn)

This work was supported in part by the Basic Research Fund of Heilongjiang University, Heilongjiang, under Grant kjck201806.

ABSTRACT In mechanical fault diagnosis of the high voltage circuit breakers (HVCBs), it is often expected that the fault type should be confirmed in time to avoid delaying the best time for mechanical fault diagnosis. The traditional diagnosis method of HVBC is not so profound for the identification of slight faults and does not consider the impact of the recall rate of fault samples on the fault diagnosis results. In this paper, we propose a method for HVCBs mechanical fault diagnosis utilizing variational mode decomposition (VMD) based on improved time segment energy entropy (ITSEE) and a new hybrid classifier. Firstly, the signal is decomposed into K intrinsic mode functions (IMFs) via VMD to establish a component matrix. Secondly, the ITSEE method is used to calculate the energy entropy of the matrix in time domain and frequency domain, so as to better extract the features of slight fault types. Finally, an optimal hybrid classifier model combined of one-class support vector machine (OCSVM) and probabilistic neural network (PNN) is used to identify four types of vibration signals of HVCBs. The experimental results show that the accuracy of unknown samples is 98.75%, and the recall of fault type is 100%. The experimental results show the effectiveness of the method and have important application value for the diagnosis of HVBCs.

INDEX TERMS High voltage circuit breakers, mechanical fault diagnosis, variational mode decomposition, improved time segment energy entropy, one-class support vector machine, probabilistic neural network.

I. INTRODUCTION

High voltage circuit breaker is an important switch device which has the dual functions of protecting the power system. However, the faults of HVCBs occurred constantly, which in economic losses [1]–[3]. An inquiry about HVCB faults by the International Council on Large Electric Systems (CIGRE) showed that the operating mechanism fault accounts for 61% [4]. Specifically, 39% of minor faults and 44% of major faults are caused by a decrease in mechanical performance [5], [6]. Such as mechanism jam, loose screws, insufficient lubrication causes time delay and insufficient spring energy storage, etc., [5], [7]–[11]. Therefore, it is of great significance to study the fault diagnosis of HVCBs. Because the mechanical vibration signal usually contains a lot of important information related to the motion state of HVCBs, it's considered to be one of the most useful tools for HVCB mechanical fault diagnosis in the past decade [12], [13].

In view of the nonlinear characteristics of the vibration signal of the circuit breaker, the time-frequency analysis method is generally used for processing. Wavelet transform (WT) [14], [15] can be regarded as an adjustable window Fourier transform (FT) [16], [17], but wavelet basis functions are often difficult to choose. Wavelet packet decomposition (WPD) has been proved that there are energy leakage problems [18], [19]. Huang *et al.* [20] empirical mode decomposition (EMD) for time-frequency analysis of HVCB vibration signals. However, the EMD method has serious modal aliasing and is susceptible to endpoint effects [21]–[23].

The associate editor coordinating the review of this manuscript and approving it for publication was Moussa Boukhnifer.

The ensemble empirical mode decomposition (EEMD) proposed by Zhang and Zhou [24] to solve the of EMD effectively. Li *et al.* [25] used LMD to decompose high-voltage circuit breaker signals. However, in practical applications, LMD sometimes also suffers the same mode mixing shortcomings as EMD does [26]. Lin *et al.* [27] improved the EMD method and proposed an iterative filtering (IF) algorithm. However, for non-stationary and non-linear signals, waveform distortion and poor adaptability are easy to occur. Motivated by the above considerations, VMD [28]–[33] method is applied in signal analysis of HVCBs in this paper. The VMD method has a solid theoretical foundation and good noise robustness [22]. So the superior performance of VMD is quickly accepted in the field of vibration signal decomposition.

At present, the following methods are generally used to extract the mechanical fault features of HVCBs. For example, VMD energy entropy [32], [34], empirical wavelet transform (EWT) [15], [35], time-domain segmentation (TDS) [5], time frequency entropy (TFE) [15], [35], fuzzy entropy [36], wavelet time frequency entropy (WTFE) [15], time segment energy entropy (TSEE) [37], envelope equal energy segmentation energy entropy (EEESEE) [38], local singular value decomposition (LSVD) [14] and envelope equal time segmentation energy entropy (EETSEE) [39]. Huang *et al.* [37] used TSEE method to extract features of HVCBs, which can distinguish delay fault types well. But the frequency domain features ignored in TSEE to a degree. Although, EETSEE method is adopted in [39] can describe the frequency domain features of the signal well, the time domain features are ignored in EETSEE to a certain extent. Combining the advantages of TSEE and EETSEE methods, this paper an improved time segmentation energy entropy (ITSEE) feature extraction method. This method can calculate the energy entropy of component matrix in the time domain and frequency domain at the same time, and extract the features of HVCB vibration signal comprehensively.

In the research of mechanical fault diagnosis, the most widely used pattern recognition methods are artificial neural networks (ANN) and support vector machines (SVM), which have been studied and applied for several years. At the same time, deep learning and transfer learning methods are gradually applied in fault diagnosis [40]–[43]. The convergent rate of back propagation neural network (BPNN) is slow, and the training time of BPNN is long. SVM is used to deal with classification problems with small training sample sets [32], [34]. But the penalty factor and kernel function parameters of the SVM method are difficult to determine either. Shao *et al.* [41] proposed a new method based on enhanced deep gated recurrent unit (GRU) and complex wavelet packet energy moment entropy for bearing fault prediction. Han *et al.* [42] proposed a novel deep adversarial convolutional neural network (DACNN) which integrates the adversarial learning framework into convolutional neural network, is proposed for intelligent fault diagnosis of mechanical systems. However, in the field of HVCB fault diagnosis, more practice is needed to verify the applicability of the above two methods. In practical applications, it is difficult to obtain a large number of vibration signal samples due to the few operation of HVCB. PNN was used for mechanical fault diagnosis of HVCBs, which showed superior classification performance under the condition of small sample data [44]–[46]. The OCSVM classifier model has been adopted to identify mechanical faults in HVCBs in [17], which can detect unknown fault categories outside the test set. Based on the above analysis, in this paper, a parameter optimized OCSVM-PNN hybrid classifier is proposed to identify mechanical vibration signal types of HVCBs. Considering that the parameters of the classifier also have some influence on the fault diagnosis results. Therefore, on the basis of k-fold cross validation [32], the optimal parameters of OCSVM and PNN classifier are determined by grid search (GS) optimization and loop traversal methods.

The main contribution of this paper is to propose: 1) a new method of ITSEE feature extraction based on VMD signal decomposition. The feature extraction method can well solve the problem that the slight fault type signal and the normal signal are easy to be confused and difficult to distinguish. 2) a new hybrid classifier of OCSVM-PNN. This method not only has high recognition accuracy, but also pays attention to the recall of fault samples, which solves the malpractice of huge economic loss caused by mistaking fault samples as normal samples. To our knowledge, this study is the first in the literature to explore the superiority of the fault sample recall for fault diagnosis. Firstly, using VMD to decompose HVCB signals into a series of IMFs with physical significance. Secondly, in order to distinguish the slight fault signal from the normal signal, the ITSEE feature extraction method is used to simultaneously extract the features of signal in time and frequency domains, and calculate the energy entropy of component matrix. Finally, the OCSVM-PNN hybrid classifier with optimal parameters is used for fault diagnosis and all fault types are correctly identified. By analyzing and comparing the fault data of HVCB, the new method proposed in this paper can not only ensure the accuracy of recognition results, but also improve the recall of fault signal samples. And the experimental results show the effectiveness of the new method.

II. RELATED WORK

A. VIBRATION DATA ACQUISITION

The experiment adopts ZW-12G/630-20 (Yueqing Wei Chuan Electric Co., Ltd., Zhejiang, China) type vacuum HVCB as the analysis object. The vibration signal was collected using a LC0159 piezoelectric acceleration sensor (Lance Technologies Inc., Hebei, China). NI USB6002 data acquisition card is used to record the data and convert the analog signals into digital signals. The maximum sampling rate of 50 kS/s. LabVIEW [30], [47], [48] software to write the signal acquisition system. In addition, AFT-0931 signal conditioner, trigger circuit and DC voltage-stabilized power also play crucial roles in supplying to build HVCB vibration signal

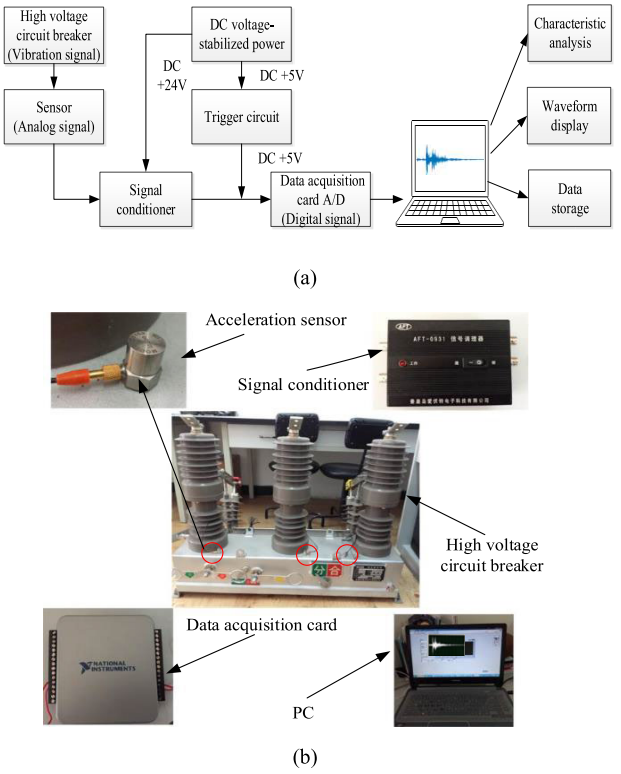

FIGURE 1. **The vibration signal acquisition system of HVCB. (a) overall framework of the system; (b) main hardware diagram.**

acquisition system. Fig. 1 shows the circuit breaker vibration signal data acquisition system.

B. FAULT DIAGNOSTIC PROCESS

The new mechanical fault diagnosis method proposed in this paper consists of four steps: data acquisition, signal decomposition, feature extraction, and fault identification. Fig. 2 shows the specific process of the fault diagnosis method. The vibration data collected by HVCB is decomposed into different modal numbers by VMD, and then the component matrix is divided. In order to make the slight fault feature more obvious, then the ITSEE method is used for feature extraction. In fault recognition, OCSVM only detects normal samples and makes corresponding decisions. For abnormal samples, OCSVM treats them as abnormal points. The anomaly samples detected by OCSVM are taken as PNN test samples. Finally, using optimized OCSVM-PNN hybrid classifier to identify the specific fault type.

III. METHODS AND TECHNIQUES

A. OVERVIEW OF VMD METHOD

VMD is a new adaptive signal decomposition method proposed by Dragomiretskiy and Zosso in 2014 [28]. Searching the optimal solution of the variational model by the method of continuous iteration, the frequency center and bandwidth of each IMF component can be continuously updated. Finally, VMD signal decomposition algorithm can be divided into the construction and solution of constrained variational problem.

Assume that each mode component is a finite bandwidth with a center frequency ω_k and the original f_t is decomposed into K IMF components. The corresponding constrained variational model is expressed as follows:

$$\begin{cases} \min\limits_{\{u_k\},\{w_k\}} \left\{ \sum\limits_{k=1}^{K} \left\| \partial_t \left[\left(\delta(t) + \frac{j}{\pi t} \right) * u_k(t) \right] e^{-j\omega_k(t)} \right\|^2 \right\} \\ s.t. \sum\limits_{k=1}^{K} u_k(t) = f(t) \end{cases} \tag{1}$$

where $*$ represents convolution, $u_k(t)$ is the mode function, ω_k is the corresponding center frequency, K is the number of modes, $\left(\delta(t) + \frac{j}{\pi t} \right) * u_k(t)$ represents analytic signal of $u_k(t)$.

To obtain the optimal solution of the (1), the following augmented Lagrange function is introduced:

$$\begin{aligned} &L(\{u_k\}, \{\omega_k\}, \lambda) \\ &= \alpha \sum_{k=1}^{K} \left\| \partial_t \left[\left(\delta(t) + \frac{j}{\pi t} \right) * u_k(t) \right] e^{-j\omega_k(t)} \right\|^2 \\ &\quad + \left\| f(t) - \sum_{k=1}^{K} u_k(t) \right\|_2^2 + \left\langle \lambda(t), f(t) - \sum_{k=1}^{K} u_k(t) \right\rangle \end{aligned} \tag{2}$$

where α is the quadratic multiplication factor, $\lambda(t)$ is the Lagrange multiplier.

The alternate direction method of multipliers is adopted to solve the saddle point of the above augmented Lagrange function, while $u_k^{n+1}, \omega_k^{n+1}, \lambda^{n+1}$ are alternately updated. The updates of $u_k^{n+1}, \omega_k^{n+1}, \lambda^{n+1}$ can be written as:

$$\hat{u}_k^{n+1}(\omega) = \frac{\hat{f}(\omega) - \sum\limits_{i \neq k} \hat{u}_i(\omega) + \frac{\hat{\lambda}(\omega)}{2}}{1 + 2\alpha(\omega - \omega_k)^2} \tag{3}$$

$$\omega_k^{n+1} = \frac{\int_0^\infty \omega \left| \hat{u}_k(\omega) \right|^2 dw}{\int_0^\infty \left| \hat{u}_k(\omega) \right|^2 dw} \tag{4}$$

$$\hat{\lambda}^{n+1}(\omega) = \hat{\lambda}^n(\omega) + \tau \left[\hat{f}(\omega) - \sum_{k=1}^{K} \hat{u}_k^{n+1}(\omega) \right] \tag{5}$$

where symbol ^represents Fourier transform, the mode $\hat{u}_k^{n+1}(t)$ can be obtained as the real part of the inverse Fourier transform of $\hat{u}_k^{n+1}(\omega)$.

In summary, the steps of the VMD algorithm are given as follows:

(1) Initialize $\hat{u}_k^1, \omega_k^1, \hat{\lambda}^1$, and n;

(2) Update u_k and ω_k according to Equations (3) and (4);

(3) Update λ according to Equation (5);

(4) Repeat the iteration above, for a given $e > 0$, if the criterion

$$\frac{\sum\limits_{k=1}^{K} \left\| \hat{u}_k^{n+1} - \hat{u}_k^n \right\|_2^2}{\left\| \hat{u}_k^n \right\|_2^2} < e \tag{6}$$

is satisfied, then stop iteration and output the results of K narrow band IMF components, else return to step (2).

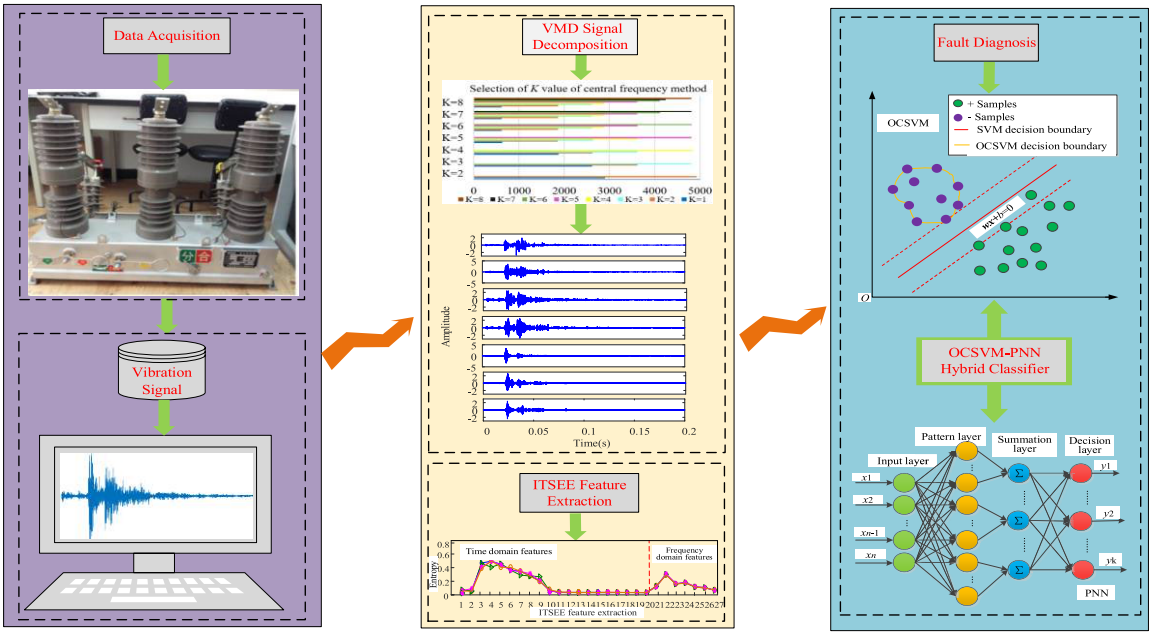

FIGURE 2. The specific process of the fault diagnosis method.

TABLE 1. Parameters of the simulated vibration signal.

Vibration Event	α_i	t_i /ms	A_i	f_i /Hz
x_1	85	15	0.1	1200
x_2	90	25	0.2	4500
x_3	70	35	0.35	5000
x_4	50	55	0.55	3000
x_5	65	45	1.0	6500

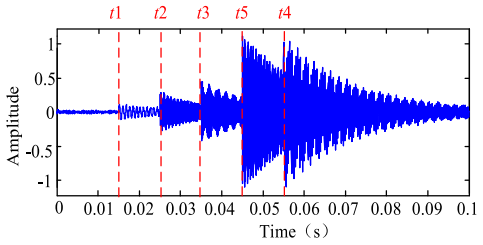

FIGURE 3. Simulated time domain waveform of vibration signal.

1) SIMULATION SIGNAL DECOMPOSITION BASED ON VMD

The vibration signal of high voltage circuit breaker consists of a series of vibration events. If the vibration generated by the motor action is not considered, the vibration event process is regarded as exponentially decaying sinusoidal signals, then the composite signal can be described as [35]:

$$X(t) = \sum_{i=1}^{n} A_i e^{-\alpha_i (t-t_i)} \sin\left(2\pi f_i (t-t_i)\right) u(t-t_i) \quad (7)$$

where is the number of vibration events, $u(t)$ is the unit step signal, t_i is the starting time of each vibration component, A_i is maximum amplitude of the i-th vibration event, f_i is the main frequency of each vibration component, α_i is the attenuation coefficient of the amplitude. The parameter of the simulation signal is shown in Tab. 1.

The simulated vibration signal is simulated by Matlab 2018 and 4000 sampling points are collected in total, sampling frequency is set to 40kS/s, sampling time is set to 0.1s. The composite vibration signal is shown in Fig. 3. The number of sub-vibration events is 5, and t1-t5 in the figure are the start times of 5 vibration events.

In mechanical fault diagnosis, signal decomposition methods such as WT [14], [15], IF [27], EMD [21], [23], [37], LMD, and EEMD [24] have been effectively applied. The pros and cons of each method have been discussed in detail in the Introduction section. Here, we decompose the simulation vibration signal (the signal in Fig. 3). Mainly analyze the vibration events of VMD and the original vibration signal, as shown in Fig. 4. In addition, the performance of VMD is also compared with IF, EMD, LMD, and EEMD methods. The original vibration events and IMF decomposed by these four methods are shown in Fig. 5.

By comparing the degree of correlation between each mode and the original vibration event, the performance of each signal processing method can be determined. When $K = 5$, the five IMFs decomposed by the VMD method are similar to the five vibration events of the original signal in Fig. 4(a). This indicates that the signal decomposed by VMD is closer to the original signal with better fidelity, and the decomposed IMF is less, which means the speed is fast and the distortion of the signal is reduced. In other words, the VMD method can completely decompose the vibration signal, which has good

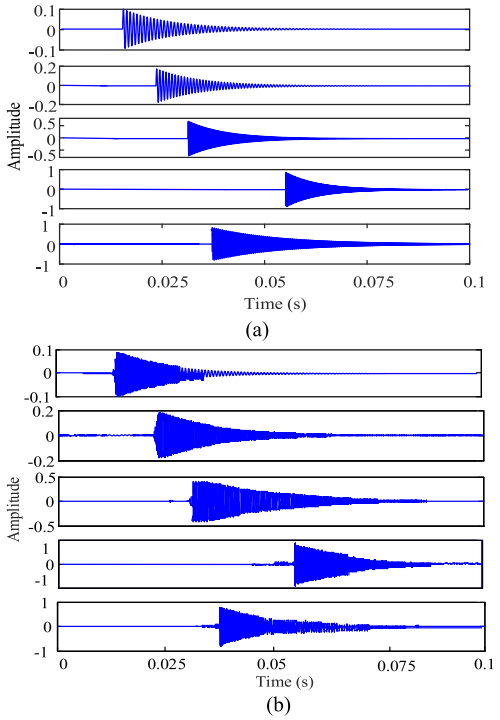

FIGURE 4. Signal decomposition. (a) Vibration components of simulation signal; (b) IMFs decomposed by VMD.

physical meaning. Therefore, the VMD method is an effective tool for time-frequency analysis of HVCBs.

Conversely, the number of IMFs we obtained through IF, EMD, LMD and EEMD methods are more than the original IMF numbers, especially EMD, LMD and EEMD. In Fig. 5(a), the IF is decomposed into 6 IMFs. Among them, the first mode contains several components that differ in frequency, the last one is the trend and the other modes are actual IMFs. Fig. 5(b), Fig. 5(c) and Fig. 5(d) shows that the number of IMFs decomposed by EMD, LMD and EEMD is often more than the number of original vibration events. Although IF performs better in overcoming singular point sensitivity, IF has almost the same performance as EMD. Among them, EMD decomposes the signal into 10 IMFs. Not only are the number of iterations increased, but also the mode aliasing problem appears in the IMFs, especially for the third mode. The LMD is decomposed into 9 IMFs. Although LMD is better than EMD in terms of end effect suppression. In this study, LMD is similar to EMD, and it also has some disadvantages of EMD algorithm. EEMD can alleviate the modal aliasing caused by EMD to a certain extent. However, EEMD decomposes the signal into 12 IMFs, which is much larger than the number of original vibration events. It can be seen that the characteristics (such as spectrum) of each mode obtained by IF, EMD, LMD and EEMD are unclear or untrue to some extent. VMD also has a shortcoming, there is no unique measurement standard in the selection of K value. Even so, it does not affect the superior decomposition performance of the VMD method. In summary, VMD has excellent decomposition characteristics for processing nonperiodic vibration signals. Therefore, the VMD method is used to process the measured signal of HVCBs in this paper.

2) DETERMINING THE NUMBER OF K MODES OF VMD

When using VMD for signal decomposition, the parameter K needs to be determined in advance. Termination of the number of modes according to the approach degree of the center frequency [49]. When the center frequency between the two modal functions is close to each other, it is considered that there is over-decomposition. Taking a measured signal of a normal condition as an example, the central frequency variation of each mode can be obtained by VMD decomposition under different K. Fig. 6 is the determination of modal number by VMD method.

As can be seen from Fig. 6, more modal components with similar center frequencies appear when K is taken as 8, which means that there is phenomenon of over-decomposition [35]. Therefore, in this paper, the number of modal components K of VMD signal decomposition is taken as 7, that is, $K = 7$.

B. FEATURE EXTRACTION BY IMPROVED TIME SEGMENT ENERGY ENTROPY METHOD

According to the energy distribution of the modal components decomposed by VMD, the energy distribution features of each sub-event are added on the basis of the time segment energy entropy (TSEE) [37] feature extraction method. The energy entropies in time and frequency domains are respectively calculated to increase the discrimination of slight fault signal features. The specific steps of the improved time segment energy entropy (ITSEE) feature extraction method is given as follows:

(1) The original multi-component signal $s(t)$ to obtain a series of modal components with real physical meanings $f_k(t)$.

(2) The component matrix is composed of the modal component $f_k(t)$. The number of rows of the component matrix is the number of modal components. The number of columns of the component matrix is the length of the modal function signal (ie, the number of sampling points). Fig. 7 show the component matrix of a normal state signal decomposed by VMD.

(3) For the measured signal, according to the duration of the signal and the validity of feature, the component matrix is divided into 20 segments along the time axis. Then, 20 matrices can be obtained, which contains 7 time-frequency blocks respectively.

(4) Normalize the energy $E_{i,j}$ of all time-frequency block $B_{i,j}(i = 1, 2, \cdots, 7; j = 1, 2, \cdots, 20)$ to the interval [0,1]. Let E be the energy of the whole component matrix. The normalization equation is defined as follows:

$$e_{i,j} = E_{i,j}/E \tag{8}$$

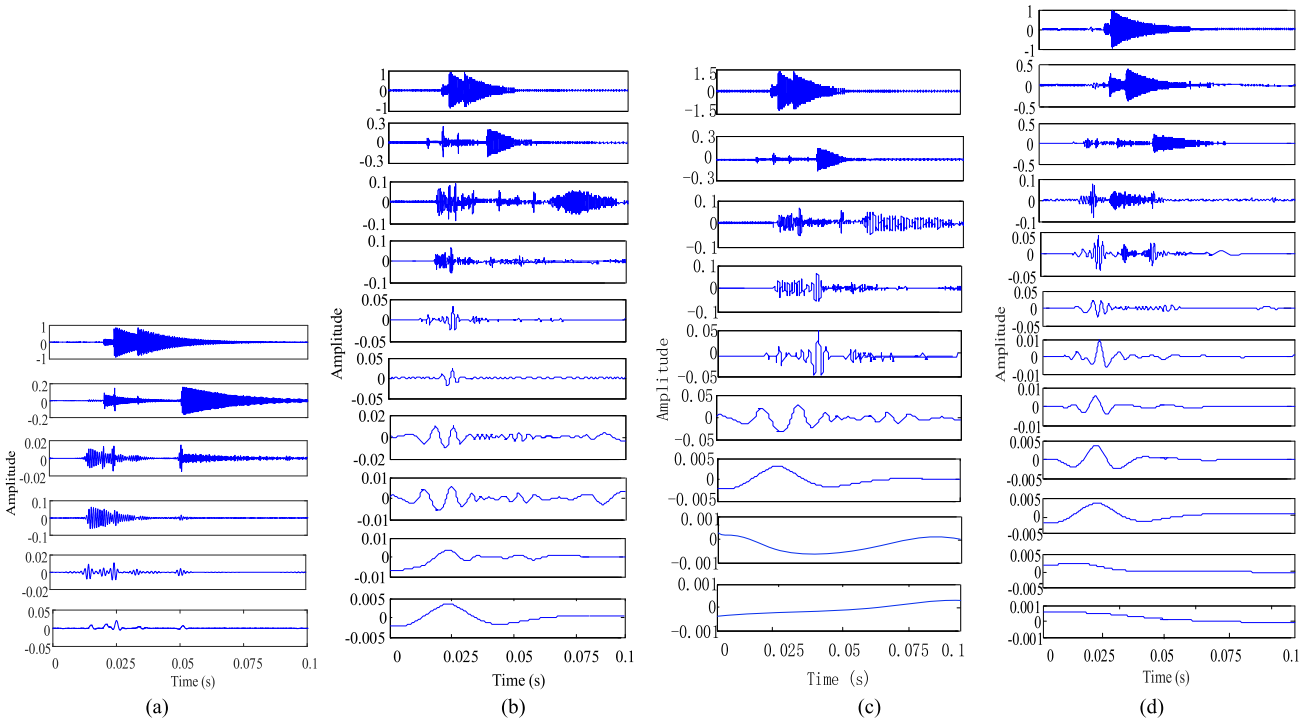

FIGURE 5. Comparison of signal decomposition. (a) IMFs decomposed by IF; (b) IMFs decomposed by EMD; (c) IMFs decomposed by LMD; (d) IMFs decomposed by EEMD.

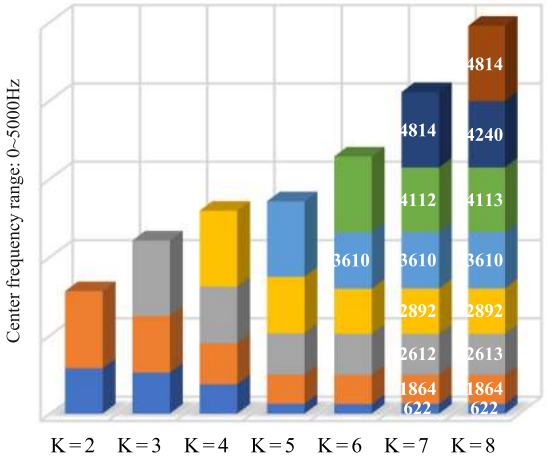

FIGURE 6. Selection of VMD modal number.

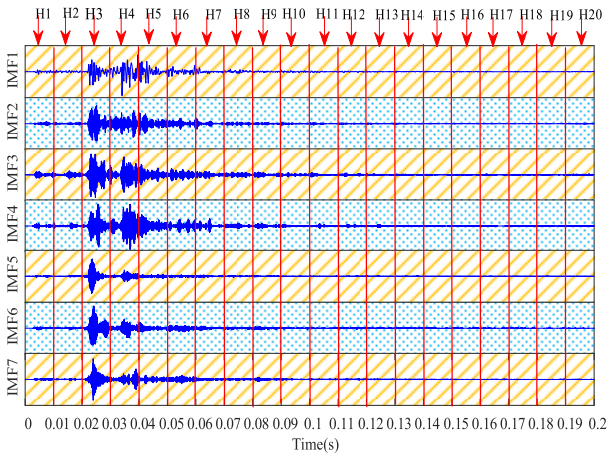

FIGURE 7. Component matrix and it's time segmentation.

(5) With H_j as a part of the signal feature energy distribution (time segment energy entropy), the following can be obtained from the basic information entropy theory:

$$H_j = -\sum_{i=1}^{7} e_{i,j} \cdot \log e_{i,j} \quad j = 1, 2, \cdots, 20 \tag{9}$$

(6) If $E_i (i = 1, 2, \cdots, 7)$ is the total energy of each subevent, then, with Q_i as another part of the signal feature energy distribution (frequency segment energy entropy):

$$Q_i = E_i / E \tag{10}$$

(7) Therefore, the ITSEE method is expressed as:

$$\boldsymbol{I_v} = [H_1, H_2, \cdots, H_{20}, Q_1, Q_2, \cdots, Q_7] \tag{11}$$

I_v is used as the input vector of OCSVM-PNN hybrid classifier to diagnose HVCBs faults. It is worth noting that in order to reflect the energy distribution of each IMF component, step (6) is the newly added feature sequence on the basis of TSEE, i.e., ITSEE.

C. OCSVM AND PNN HYBRID CLASSIFIER

1) OCSVM

Different to SVM, OCSVM [17] is a classifier that only recognizes certain categories of interest, which is

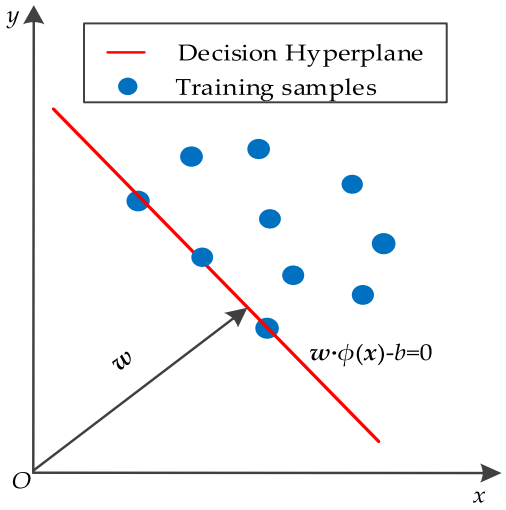

FIGURE 8. The principle of OCSVM.

applicable to the field where it is difficult to obtain negative samples. Considering the characteristics of HVCB fault samples of difficult to obtain, OCSVM is adopted which can detect abnormal samples well and ensure recall of abnormal samples.

Let $X = [x_1, x_2 \cdots, x_n] \in R^{n\times m}$ be the training data set, then X contains $n\times m-$ dimensional feature vectors extracted.

The principle of OCSVM shown in Fig. 8. The kernel function is needed in OCSVM to map the original low-dimensional feature space $R^{n\times m}$ to the high-dimensional feature space H: $x_i \rightarrow \phi(x_i)$ then a high-dimensional space hyperplane $w \cdot \phi(x_i) - b = 0$ is established. It is necessary to solve the quadratic programming problem as shown in (12) and (13).

$$\min F(w, b, \xi_i) = \frac{1}{2}\|w\|^2 + \frac{1}{vn}\sum_{i=1}^{n}\xi_i - b \tag{12}$$

$$s.t.\ (w \cdot \phi(x_i)) \geq b - \xi_i, \quad \forall i, \xi_i \geq 0\ i = 1, 2, \cdots n \tag{13}$$

where w and b represent the normal vector and the intercept of the hyperplane respectively, ξ_i is the slack variable, the error limit $v \in (0, 1)$ is used to control the upper of the outliers number in the training set, x_i is a m-dimensional eigenvector.

To solve the quadratic programming problem, the Lagrange function is given as follows:

$$\begin{aligned} L(w, \xi, b.a, \beta) &= \frac{1}{2}\|w\|^2 + \frac{1}{vn}\sum_{i=1}^{n}\xi_i \\ &\quad - \sum_{i=1}^{n}\alpha_i((w \cdot \phi(x_i)) - b + \xi_i) - \sum_{i=1}^{n}\beta_i\xi_i \end{aligned} \tag{14}$$

where $a_i \geq 0$ and $\beta_i \geq 0$ are Lagrange multipliers.

Taking the partial derivatives of variables w, ξ_i and b, and making them equal to zero. The following Equations can be obtained:

$$w = \sum_{i=1}^{n}\alpha_i\phi(x_i) \tag{15}$$

$$\sum_{i=1}^{n}\alpha_i = 1 \tag{16}$$

$$\alpha_i = \frac{1}{vn}\beta_i \tag{17}$$

By simplifying the above equations, the following dual problems can be obtained:

$$min\ \frac{1}{2}\sum_{i=1}^{n}\sum_{j=1}^{n}\alpha_i\alpha_j K(x_i, x_j) \tag{18}$$

$$s.t.\ 0 \leq \alpha_i \leq \frac{1}{vn}, \quad \sum_{i=1}^{n}\alpha_i = 1 \tag{19}$$

where $K = (x_i, x_j) = f(x_i)f(x_j)$ is the kernel function.

Finally, the classification decision function of OCSVM is calculated by:

$$f(x) = sgn\left(\sum_{i=1}^{n}\alpha_i K(x_i, x) - b\right) \tag{20}$$

where $b = \sum_{i=1}^{n}\alpha_i K(x_i, x_j)$, $\mathrm{sgn}(x)$ represents the sign function.

For a given test sample z, the OCSVM function is used for decision making. If f_z is greater than 0, the test sample will be judged as the target sample. Conversely, it will be judged as the non-target samples.

2) PNN

PNN was proposed by D.F. Specht in 1989 [44], which developed from the radial basis function neural network (RBFNN). The most important advantage of PNN is that the training of network is easy and instantaneous [50]. Besides, the sparse samples are adequate for network performance. PNN is a four-layer feed-forward neural network [45], i.e., input layer, pattern layer, summation layer and decision layer (or output layer). The network structure is shown in Fig. 9.

Assuming that an input vector to be classified is $X = [x_1, x_2 \cdots, x_n]$ for input layer. The number of neurons in the pattern layer is the same as the number of training samples.

The summing layer simply sums the outputs of the training samples of the same category in the pattern layer, so the connection mode of the network here is not a full connection. The decision layer is $Y = [y_1, y_2 \cdots y_k]$ and its output is binary output. That is, the corresponding position of the output layer will output 1, otherwise 0.

3) CLASSIFIER PERFORMANCE INDEXES

Generally, the categories we focus on are positive and the other categories are negative, so the results of the classifier on the test datasets will have four cases. Tab. 2 is an

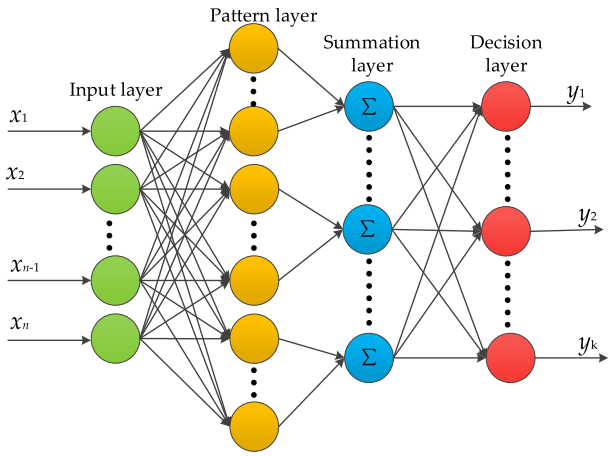

FIGURE 9. The structural diagram of probabilistic neural networks.

TABLE 2. Obfuscation matrix.

Actual	Predic	
	Positive examples	Negative examples
Positive examples	TP (True Positive)	FN (False Negative)
Negative examples	FP (False Positive)	TN (Ture Negative)

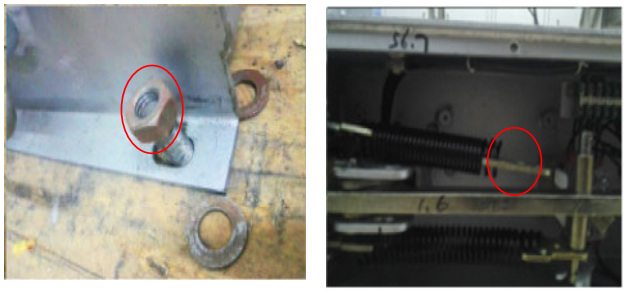

FIGURE 10. Simulation of (a) Fault I and (b) Fault III.

obfuscation matrix. TP means for the number of the true positive samples. FP stands for the number of the false positive samples. FN means for the number of the false negative samples. TN stands for the number of the true negative samples.

In the field of machine learning, the indicators commonly used to measure the classifier performance include accuracy, recall etc. These indexes are applicable to the evaluation of classification problems.

Accuracy is the ratio of the number of samples correctly identified by the classifier to the total number of samples in the test set. The formula for calculation is as follows:

$$Accuracy = \frac{TP + TN}{TP + FN + FP + TN} \tag{21}$$

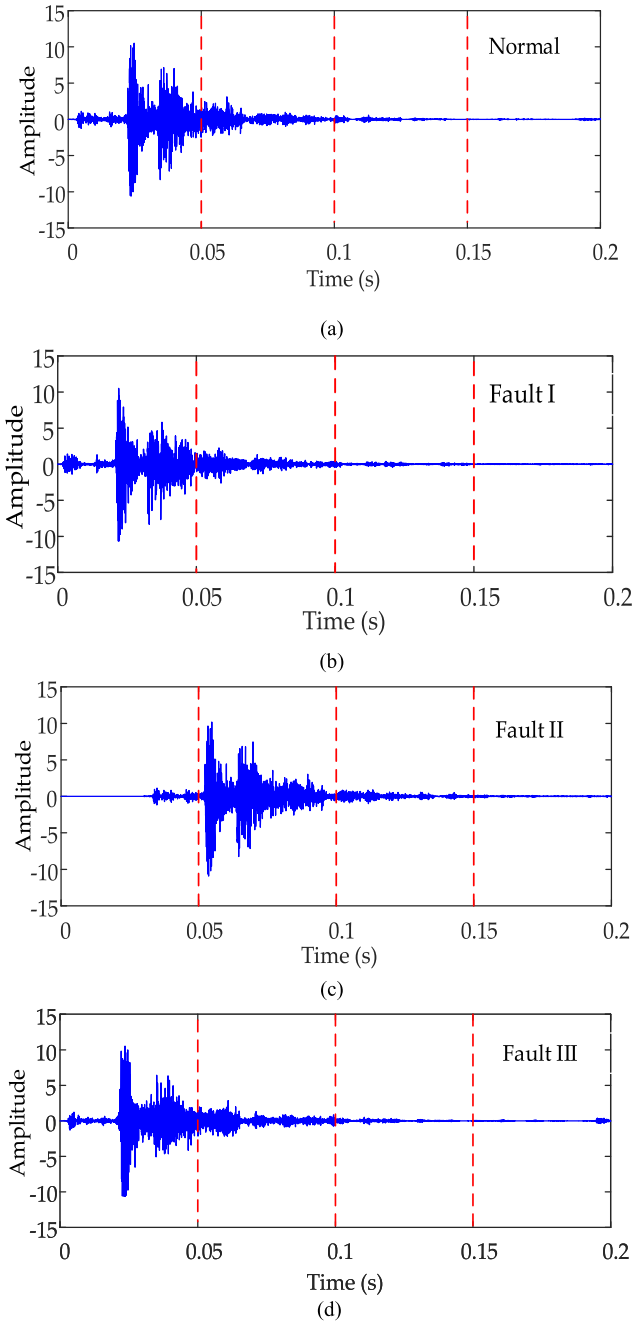

FIGURE 11. Time domain waveform of vibration signal (a) Normal state; (b) base screw looseness; (c) delayed action; (d) the energy storage spring shedding.

Recall indicate how many positive categories in the sample are correctly predicted. The definition is as follows:

$$Recall = \frac{TP}{TP + FN} \tag{22}$$

IV. EXPERIMENTAL RESULTS AND ANALYSIS

According to the common mechanical faults of circuit breakers, three types of mechanical faults are simulated experimentally: base screw looseness (Fault I), delayed action (Fault II), the buffer spring shedding (Fault III). The simulated Fault I

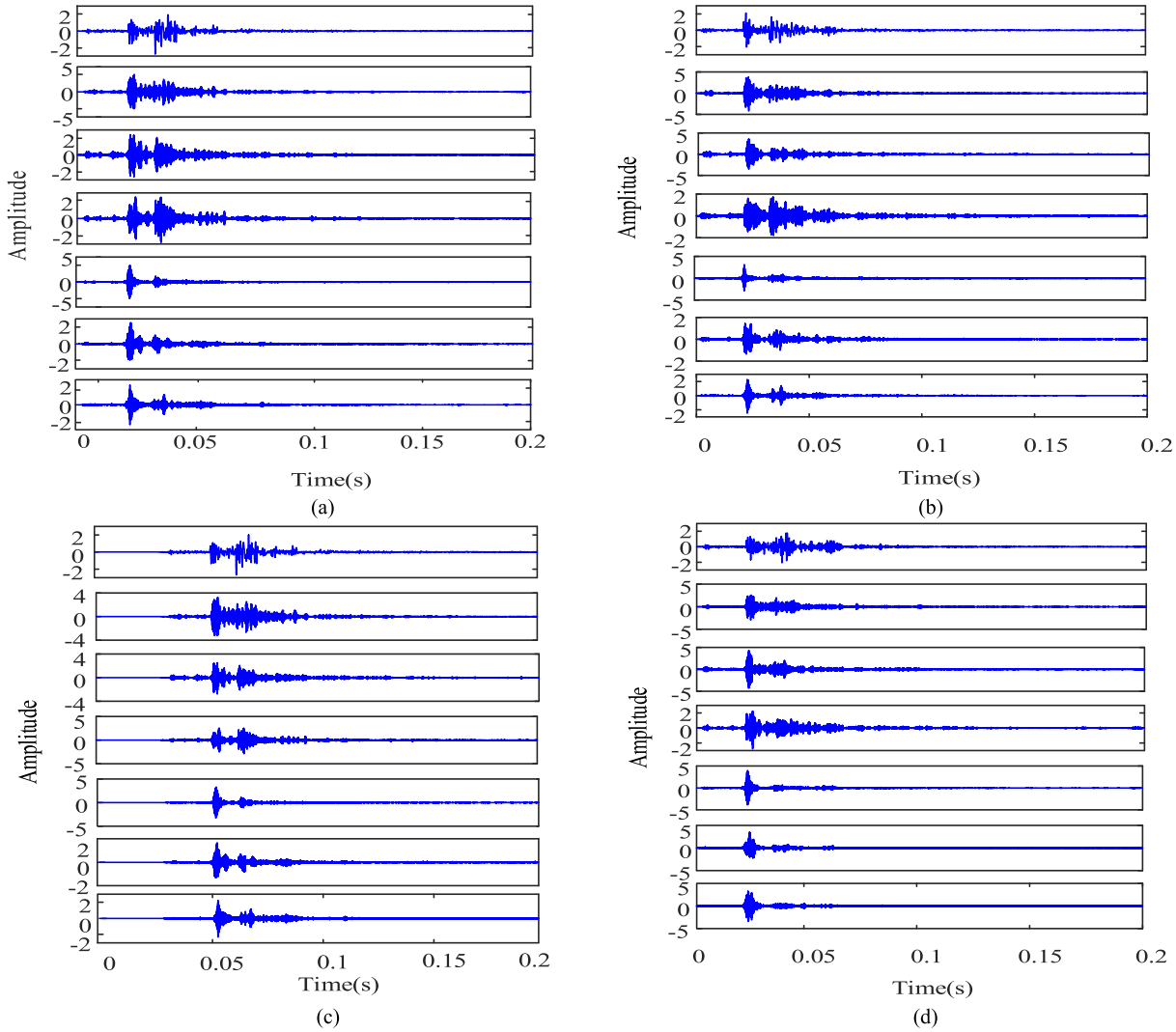

FIGURE 12. Decomposition of measured signals by VMD method (a) Normal; (b) Fault I; (c) Fault II; (d) Fault III.

and Fault III are shown in Fig.10 (a) and (b). Among them, the delay fault (Fault II) is mainly caused by the delay action of the electromagnetic mechanism of the circuit breaker or the insufficient lubrication and jamming of the operating mechanism.

Through the data acquisition system, the vibration signal samples in the normal state and the three fault states are collected respectively, with 50 groups each state. The waveforms of four different types of original vibration signals are shown in Fig. 11. The sampling frequency is 40 Ks/s and the sampling time is 0.2s. It can be seen intuitively from Fig. 11 that the time domain waveforms of normal state and Fault II are very similar except that there is a time delay. Normal state is different from Fault I and Fault III in instantaneous frequency and instantaneous amplitude. The main reason for these differences is due to the change of mechanical components in the process of impact or friction when a fault occurs.

A. SIGNAL DECOMPOSITION

According to the previous chapter, the number of modes of VMD is $K = 7$, and other parameters are set as default values. Inputting four types of vibration signal data, and VMD signal decomposition is shown in Fig. 12.

From the output results of VMD in Fig. 12, it can be seen that the amplitude modulation and frequency modulation subcomponents of vibration signals of the four different states are similar, but there are also some differences. For the normal signal and Fault I, the difference between them is not obvious. This is because the mechanical state of the loose screw has little influence, which belongs to slight fault (Fault I). And each mode component of normal signal is most similar to the Fault II, where the main difference is the time delay. The vibration signal of Fault II has the significant time delay compared with other types of signals. However, the modal component of the Fault III signal is more different from the other three types of signals.

TABLE 3. Frequency energy feature of ITSEE.

Signal type	Q_1	Q_2	Q_3	Q_4	Q_5	Q_6	Q_7
Normal	0.1110	0.3256	**0.1544**	0.1768	**0.1023**	0.0923	0.0402
	0.1039	0.3329	**0.1623**	0.1812	**0.1089**	0.0912	0.0412
	0.1187	0.3195	**0.1572**	0.1758	**0.1091**	0.0858	0.0457
	0.1200	0.3099	**0.1506**	0.1711	**0.1101**	0.0819	0.0497
Fault I	0.1071	0.3648	**0.2345**	0.1219	**0.0578**	0.0531	0.0621
	0.1123	0.3491	**0.2289**	0.1348	**0.0643**	0.0460	0.0578
	0.1107	0.3670	**0.2306**	0.1237	**0.0621**	0.0452	0.0607
	0.1101	0.3315	**0.2399**	0.1151	**0.0731**	0.0402	0.0657
Fault II	0.1043	0.3351	0.1581	0.1729	0.0971	0.0888	0.0581
	0.1210	0.3199	0.1659	0.1768	0.1031	0.0861	0.0468
	0.1126	0.3233	0.1575	0.1752	0.0961	0.0879	0.0473
	0.1119	0.3117	0.1465	0.1843	0.0921	0.0963	0.0659
Fault III	0.1063	0.1950	0.2688	0.1121	0.1178	0.1076	0.1191
	0.1051	0.1810	0.2467	0.1181	0.1210	0.1011	0.1083
	0.1015	0.1797	0.2561	0.1163	0.1198	0.1080	0.1186
	0.1189	0.1701	0.2541	0.1043	0.1090	0.1189	0.1274

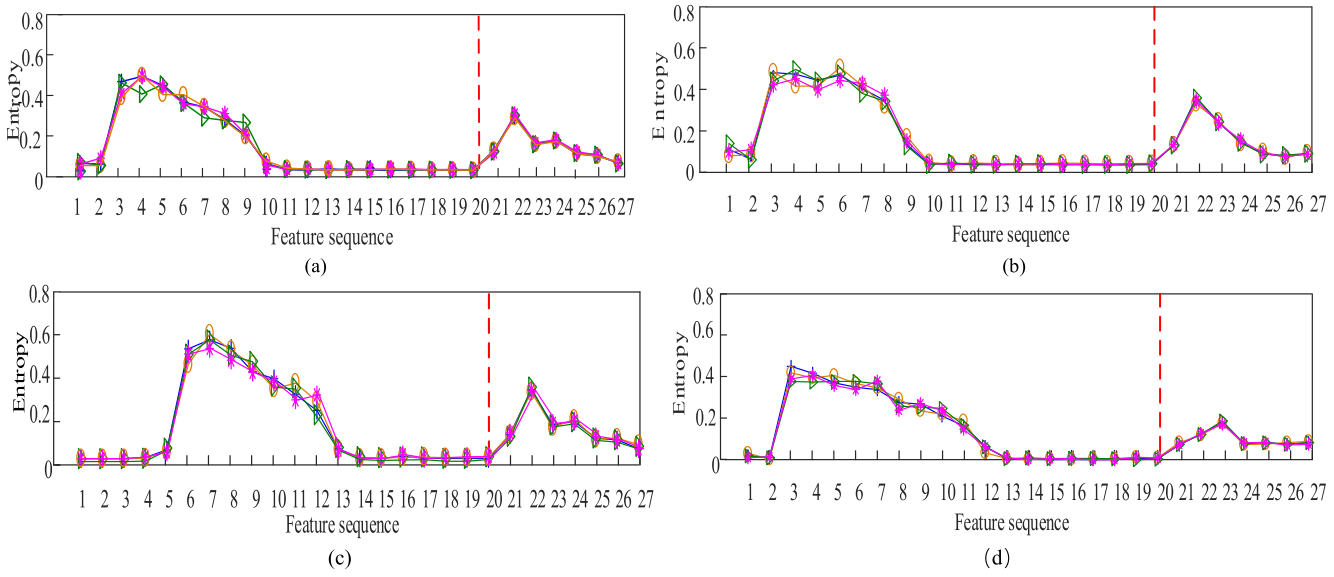

FIGURE 13. Feature curves of four types of signals. (a) Normal; (b) Fault I; (c) Fault II; (d) Fault III.

B. FEATURE VECTOR EXTRACTION AND ANALYSIS

Based on the ITSEE feature extraction method, the energy distribution features of each sub-event are added, at the same time, the signal is extracted in the time domain and the frequency domain. Tab. 3 is the energy feature entropy (Q_i) of ITSEE in the frequency segment. For clarity, each type of signal lists only four sample features. As can be seen from Tab. 3 that the four vibration signals under the same signal type have similar frequency entropy vectors, while different types of vibration signals have different values. For normal signal and Fault I, the difference between the eigenvalues of Q_3 and Q_5 are obvious, and easy to distinguish.

Fig. 13 shows the feature distribution of four mechanical vibration signals of the ITSEE method and the dimension of each feature is 20+7. The first 20 feature sequences (left side of the dotted line) are the H_i features extracted by feature extraction step (5), which reflect the energy distribution in the time domain. The last 7 feature sequences (right side of the dotted line) are the Q_i features extracted by feature extraction step (6), which reflect the energy distribution in the frequency domain.

It can be seen from Fig. 13 that the trend of characteristic curve between the same type of vibration signals is similar. While the characteristic curves of different types of vibration signals have obviously differences. The specific analysis is given as follows:

TABLE 4. VMD-energy entropy feature.

Signal type	H_1	H_2	H_3	H_4	H_5	H_6	H_7
Normal	1.3732	1.3240	1.3623	1.4153	1.1471	1.2192	1.1025
	1.3541	1.3097	1.4010	1.3985	1.1503	1.2153	1.0696
	1.3425	1.3336	1.3505	1.3806	1.2105	1.1817	1.0473
	1.3304	1.3215	1.3514	1.4106	1.1897	1.2018	1.0821
Fault I	1.4853	1.2275	1.4873	1.5281	1.2016	1.2940	1.1927
	1.5024	1.2467	1.4506	1.5302	1.2459	1.2913	1.2412
	1.4651	1.2882	1.4698	1.5133	1.1929	1.2742	1.1651
	1.5182	1.2101	1.4601	1.5368	1.2153	1.2606	1.2115
Fault II	0.9807	0.9824	0.9123	0.6638	0.5701	0.6580	0.7127
	1.0381	1.1133	0.8714	0.7216	0.5937	0.6561	0.6894
	0.9982	1.1728	0.9017	0.6839	0.5765	0.6879	0.7056
	0.9714	1.0975	0.9273	0.6943	0.5821	0.6663	0.6863
Fault III	1.7057	1.6324	1.7102	1.7491	1.4209	1.2782	1.3766
	1.6813	1.5873	1.7260	1.6806	1.3983	1.2340	1.3901
	1.6526	1.6216	1.6799	1.7328	1.4016	1.1972	1.4186
	1.6273	1.6018	1.6513	1.7552	1.3758	1.2404	1.3964

(1) Between the characteristic curves of Fault I and Normal, there is no obvious difference in the first 20 feature sequences. But the normal type of vibration signal has two peaks on the last 7 feature sequences. This is due to the fact that when mechanical failure occurs, the vibration events change as the mechanical state changes. This indicates that ITSEE can distinguish Fault I and Normal well.

(2) For Fault II and Normal, the last 7 frequency domain feature sequences are roughly consistent. But in the first 20 time-domain feature sequences, there is a significant time delay between Normal and Fault II.

(3) The first 20 feature sequences and the last 7 feature sequences of Fault III are quite different from other types of signal features. In other words, the energy distribution of Fault III along the time axis and frequency band is clearly different from the other three types of signals.

To validate the superiority of the ITSEE feature extraction method proposed in this study, we follow the feature extraction methods in the literature [32], [34], [36], and extract the VMD energy entropy and VMD fuzzy entropy of the intrinsic mode function (IMF) respectively for experimental comparison. Tab. 4 and Tab. 5 respectively correspond to the entropy values of VMD signal features. For clarity, only four data samples of each type are listed. Fig. 14 shows the feature distribution trends of VMD energy entropy and VMD fuzzy entropy for four vibration signal types. As can be seen from Fig. 14 (a), there is no significant difference in the VMD energy entropy feature distribution between the normal signal and the other three fault signals. That is, the VMD energy entropy method is difficult to distinguish the four types of signals, especially for Normal signal and Fault I (slight fault). In Fig. 14 (b), VMD fuzzy entropy feature extraction can well distinguish Fault I and Fault III signals. However, it is almost difficult to distinguish between the features of Normal signal and Fault II (delay signal). This feature can be clearly

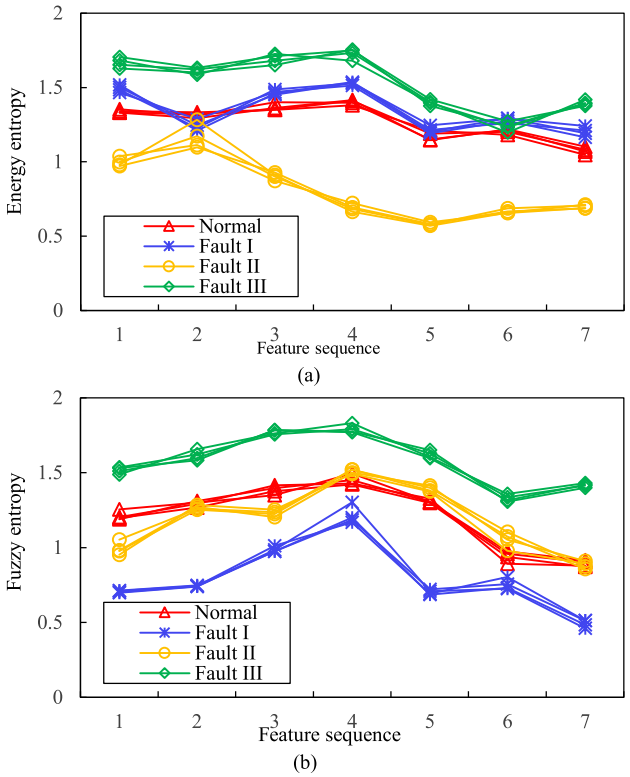

FIGURE 14. Energy entropy and fuzzy entropy feature distribution of four types of vibration signal. (a) VMD energy entropy; (b) VMD fuzzy entropy.

seen from Tab. 5 that the entropy values of Normal signal and Fault II in E_2, E_4, E_5 and E_7 are not much different. To sum up, the ITSEE feature extraction method proposed in this paper can clearly distinguish four types of signals, which verifies the effectiveness of the feature extraction method. In the following sections, we will use the four signal features

TABLE 5. VMD-fuzzy entropy feature.

Signal type	E_1	E_2	E_3	E_4	E_5	E_6	E_7
Normal	1.1882	**1.3107**	1.3983	**1.4507**	**1.3073**	0.9579	**0.9037**
	1.2026	**1.2926**	1.4156	**1.5013**	**1.3271**	0.8931	**0.8795**
	1.1968	**1.2669**	1.3763	**1.4280**	**1.2993**	0.9350	**0.8720**
	1.2550	**1.3004**	1.3504	**1.4047**	**1.3063**	0.9742	**0.9149**
Fault I	0.7017	0.7420	0.9747	1. 2002	0.6863	0.7307	0.4849
	0.7106	0.7436	1.0125	1.1691	0.6912	0.8040	0.5127
	0.6982	0.7392	0.9852	1.3024	0.7089	0.7244	0.4609
	0.7131	0.7481	0.9738	1.1853	0.7201	0.7568	0.59125
Fault II	0.9817	**1.2713**	1.2041	**1.5012**	**1.4130**	1.0535	**0.9101**
	0.9771	**1.2530**	1.2240	**1.5198**	**1.3987**	1.1042	**0.8728**
	0.9520	**1.2834**	1.2535	**1.4930**	**1.3743**	0.9785	**0.8926**
	1.0521	**1.2586**	1.2360	**1.5211**	**1.3818**	1.0742	**0.8571**
Fault III	1.5107	1.5972	1.7828	1.7701	1.5972	1.3957	1.4205
	1.5351	1.6214	1.7557	1.7907	1.6281	1.4360	1.4136
	1.4891	1.6563	1.7624	1.8310	1.6031	1.3584	1.4308
	1.5320	1.5826	1.7853	1.7745	1.6505	1.3069	1.3994

TABLE 6. OCSVM-PNN diagnosis results.

Test	Test samples	Diagnosis results				Accuracy
		Normal	Fault I	Fault II	Fault III	
Normal	20	19	1	0	0	90%
Fault I	20	0	20	0	0	100%
Fault II	20	0	0	20	0	100%
Fault III	20	0	0	0	20	100%

extracted by ITSEE method for classifier recognition and fault diagnosis.

C. FAULT DIAGNOSIS USING HYBRID CLASSIFIER OCSVM-PNN

For four types of signals, 50×4 groups of vibration data samples are collected in data acquisition. Among them, randomly select 30×4 groups as training samples, and the remaining 20×4 groups as test samples. Fig. 15 shows the diagnosis flowchart of OCSVM-PNN hybrid classifier.

In order to improve the recognition ability of OCSVM classifier to test samples, it is necessary to adjust the error limit v and the kernel function parameter g. For the actual measured signals in this paper, the 10-fold cross validation method commonly used in engineering is combined with the GS method to solve the parameter optimization problem [32].

After repeated experiments, the optimal parameter combination is $v = 0.11$ and $g = 0.01$. In the training process, the 10-fold cross validation method is used to optimize the smoothing parameters δ to improve the classification performance of PNN. The mean-square error (MSE) of the actual output and the predicted output of the classifier is averaged, and then calculate the standard deviation. Fig. 16 shows the optimization trend of PNN parameter δ. It can be seen from Fig. 16 that the mean value of MSE under the same parameter δ first rise after falling. When the mean value of MSE is the minimum value, the trend of standard deviation of MSE is relatively gentle. At this time, the optimal smoothing parameter $\delta = 1.0$, the corresponding mean value of MSE is 0.03849, and the standard deviation is 0.01986.

The classification results of OCSVM-PNN hybrid classifier are shown in Tab. 6. There is a normal sample recognized by the OCSVM-PNN classifier as the type of Fault I. Although OCSVM-PNN failed to identify all the normal samples, it has not identified fault samples as normal samples. And the accuracy of three fault types are 100%. This indicate that the fault type signal samples can all be identified under the premise of ensuring accuracy, which reduces the probability that the fault type is misdiagnosed as the normal type. That is, OCSVM-PNN hybrid classifier model can effectively identify all fault signals, especially for slight faults (Fault I), which can also be accurately classified. We select BPNN and SVM classifier to repeat the above experiment, and the comparative results are shown in Tab. 7.

As illustrated in Tab. 6 and Tab. 7, the accuracy of OCSVM-PNN classifier model for identifying Normal samples is 90%, which is significantly higher than that of BPNN and SVM classifiers. OCSVM-PNN can identify all samples of the Fault I, Fault II and Fault III. For the Fault I, the accuracy of BPNN and SVM are 85% and 90%, respectively. It can be seen that the latter two classifier models can not accurately identify samples with slight faults (Fault I). At the

TABLE 7. BPNN and SVM diagnosis results.

Classifier	Test	Test samples	Diagnosis results				Accuracy
			Normal	Fault I	Fault II	Fault III	
BPNN	Normal	20	17	2	1	0	85%
	Fault I	20	2	17	1	0	85%
	Fault II	20	1	0	19	0	95%
	Fault III	20	0	0	0	20	100%
SVM	Normal	20	17	3	0	0	85%
	Fault I	20	2	18	0	0	90%
	Fault II	20	0	0	20	0	100%
	Fault III	20	0	0	0	20	100%

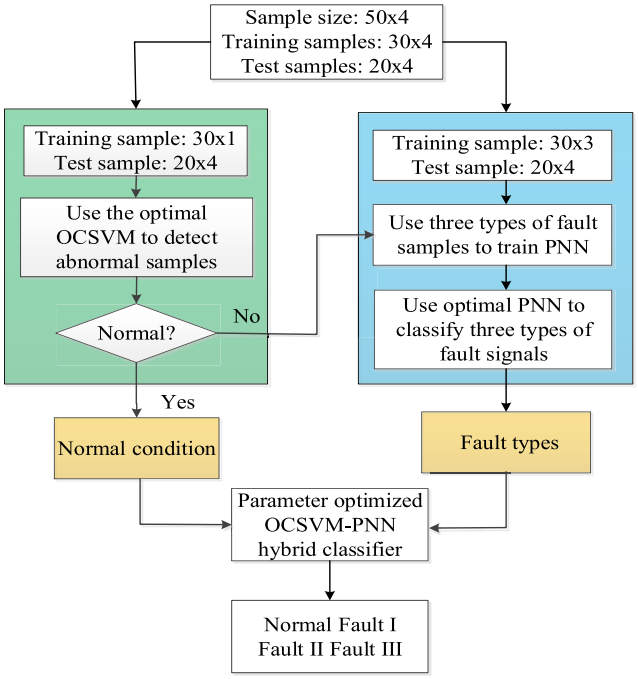

FIGURE 15. The diagnosis flowchart of OCSVM-PNN hybrid classifier.

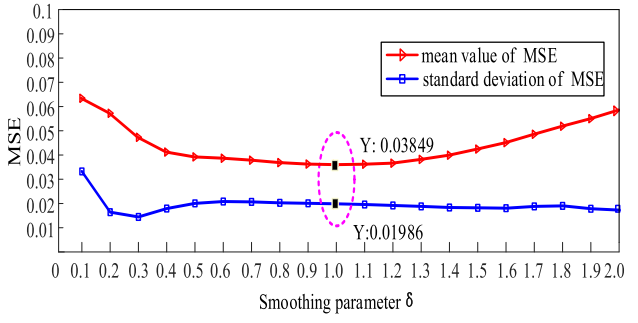

FIGURE 16. Parameter optimization of PNN.

same time, BPNN classifier is also unable to fully identify the Fault II. For mechanical fault diagnosis, it is often hoped that the fault type can be found in time to avoid delaying the optimal fault diagnosis time. Therefore, the fault diagnosis ability of OCSVM-PNN hybrid classifier is better than BPNN and SVM.

TABLE 8. The recall performance indexes of classifier.

Classifier	All types	Obfuscation matrix		Recall
OCSVM-PNN	80	60	0	1.00
		1	19	0.95
BPNN	80	56	4	0.93
		3	17	0.85
SVM	80	58	2	0.97
		3	17	0.85

In the practical application of HVCBs mechanical fault diagnosis, the loss of identifying the fault samples as normal samples is much more serious than that of identifying the normal samples as fault samples. Therefore, this paper believes that the performance of the classifier can not only focus on the accuracy, but also require a high recall rate of the signal sample recognition results. According to the confusion matrix of the recognition result, the performance index of the classifier recall rate shown in Tab. 8 is obtained.

As shown in Tab. 8, each mechanical state contains 20 samples and all fault samples are regarded as positive samples. For two different classifiers, the recall of OCSVM-PNN to Normal signal samples is 0.95, which is significantly higher than that of BPNN and SVM. The main reason for the obvious difference is that Fault I (loose base screw) is a slight fault, which is easily confused with Normal type signals. Not only can BPNN and SVM classifiers fail to correctly identify Fault I and Normal, but also the ability of BPNN to recognize Fault II is poor. For the recall of three fault signal samples, the BPNN and SVM classifiers are only 0.93 and 0.97. But the recall of OCSVM-PNN to fault signal samples reached 1.00. This shows that the OCSVM-PNN can accurately identify all fault samples and can correctly classify Normal and Fault I. It is proved that OCSVM-PNN classifier model has superior classification effect.

In order to further analyze the superiority of OCSVM-PNN hybrid classifier scheme, Tab. 9 comprehensively compares the various performance indicators of BPNN and SVM. For all test samples, the accuracy of BPNN and SVM classifiers are 91.25% and 93.75%, and the accuracy of OCSVM-PNN is as high as 98.75%, which shows the good classification ability of the hybrid classifier model. At the same time, this paper considers that the economic loss caused by identifying

TABLE 9. Comparison of model performance.

Classifier	Training samples	Test samples	Accuracy	Recall	Training time	Diagnosis time
OCSVM-PNN	120	80	98.75%	100%	1.48s	1.13s
BPNN	120	80	91.25%	93.33%	75.38s	75.06s
SVM	120	80	93.75%	96.67%	4.30s	4.18s

slight faults as normal faults is much greater than the economic losses caused by identifying normal states as fault states. Thus, compared with the BPNN and SVM classifiers, the recall of OCSVM-PNN for the three types fault samples is 100%, which can effectively detect fault signals. The OCSVM-PNN model can not only ensure accuracy, but also identify the samples of slight faults (Fault I) to the greatest extent. So as to reduce the probability of missing the best maintenance opportunity of the equipment when the slight fault is recognized as normal state. From the training time point of view, BPNN training time is the longest, which also verifies the shortcomings described by BPNN in the Introduction. The diagnosis time of OCSVM-PNN is 1.13s. Compared with BPNN and SVM classifier, OCSVM-PNN has fastest recognition speed and greatly improves the efficiency of fault diagnosis. Therefore, we can conclude that the OCSVM-PNN hybrid classifier model not only has high classification accuracy and fast speed, but also has high recall of fault samples. It has better fault detection capability and is more suitable for circuit breaker fault diagnosis which requires a higher reliability.

V. CONCLUSION

This paper presents a new method for mechanical fault diagnosis of HVCBs. The simulation and practical test results demonstrate the following advantages of the new method:

1) Compared with traditional signal decomposition (IF, EMD, EEMD), VMD can better display the characteristics of vibration signals and the decomposed modes have more clear physical meaning.

2) Based on the original feature extraction method, the ITSEE method adds the feature sequence of energy distribution in the signal frequency domain, which more effectively and comprehensively highlights the features of the signal in time and frequency domains. For example, when distinguishing Normal and Fault I type signals (slight fault), the feature sequence extracted by ITSEE method makes the features between signals more obvious.

3) OCSVM-PNN hybrid classifier model not only improves the accuracy, but also improves the recall of fault samples. Especially in the fault diagnosis of HVCBs with slight fault type (Fault I), the OCSVM-PNN hybrid classifier shows significant advantages. The hybrid classifier model can effectively reduce the probability of missing the best maintenance time because of identifying slight faults as normal types.

REFERENCES

[1] G. L. Yuan, "Analysis of an accident caused by the 10 kV breaker's failure to act in a 110 kV substation," *J. Electr. Power*, vol. 25, no. 6, pp. 493–495, Oct. 2012.
[2] M. Landry, F. Leonard, C. Landry, R. Beauchemin, O. Turcotte, and F. Brikci, "An improved vibration analysis algorithm as a diagnostic tool for detecting mechanical anomalies on power circuit breakers," *IEEE Trans. Power Del.*, vol. 23, no. 4, pp. 1986–1994, Oct. 2008.
[3] A. A. Razi-Kazemi, M. Vakilian, K. Niayesh, and M. Lehtonen, "Circuit-breaker automated failure tracking based on coil current signature," *IEEE Trans. Power Del.*, vol. 29, no. 1, pp. 283–290, Feb. 2014.
[4] C. R. Heising, A. L. J. Janssen, W. Lanz, E. Colombo, and E. N. Dialynas, "Summary of CIGRE 13.06 working group world wide reliability data and maintenance cost data on high voltage circuit breakers above 63 kV," *Proc. IEEE IAS*, vol. 3, Nov. 1994, pp. 2226–2234.
[5] J. Qi, X. Gao, and N. Huang, "Mechanical fault diagnosis of a high voltage circuit breaker based on high-efficiency time-domain feature extraction with entropy features," *Entropy*, vol. 22, no. 4, p. 478, Apr. 2020.
[6] CIGRE Working Group, "Final report of the second international enquiry on high voltage circuit breaker failures and defects in service," CIGRE Work. Group, Paris, France, VIGRE Rep. 83, 1994.
[7] S. Ma, M. Chen, J. Wu, Y. Wang, B. Jia, and Y. Jiang, "High-voltage circuit breaker fault diagnosis using a hybrid feature transformation approach based on random forest and stacked autoencoder," *IEEE Trans. Ind. Electron.*, vol. 66, no. 12, pp. 9777–9788, Dec. 2019.
[8] G. Chang, Z. Q. Zhang, and Y. Wang, "Review on mechanical fault diagnosis of high-voltage circuit breakers based on vibration diagnosis," *High Voltage App.*, vol. 47, no. 8, pp. 85–90, Aug. 2011.
[9] L. Lin and Z. Y. Chen, "Mechanical fault diagnosis of high-voltage circuit breakers based on rough set neural networks and vibration signal," *Trans. China Electrotech. Soc.*, vol. 35, no. S1, pp. 277–283, Jan. 2020.
[10] M. Mishra and P. K. Rout, "Fast discrete s-transform and extreme learning machine based approach to islanding detection in grid-connected distributed generation," *Energy Syst.*, vol. 10, no. 3, pp. 757–789, Aug. 2019.
[11] A. Janssen, D. Makareinis, and C.-E. Solver, "International surveys on circuit-breaker reliability data for substation and system studies," *IEEE Trans. Power Del.*, vol. 29, no. 2, pp. 808–814, Apr. 2014.
[12] G. Chang, Y. Wang, and W. Wang, "Mechanical fault diagnosis of high voltage circuit breakers utilizing zero-phase filter time-frequency entropy of vibration signal," *Proc. CSEE*, vol. 33, no. 3, pp. 155–162, Jan. 2013.
[13] S. T. Wan and L. Chen, "Fault diagnosis of high-voltage circuit breakers using mechanism action time and hybrid classifier," *IEEE Access*, vol. 7, pp. 85157–851461, 2019.
[14] Y.-M. Hsueh, V. R. Ittangihal, W.-B. Wu, H.-C. Chang, and C.-C. Kuo, "Fault diagnosis system for induction motors by CNN using empirical wavelet transform," *Symmetry*, vol. 11, no. 10, p. 1212, Sep. 2019.
[15] P. Liang, C. Deng, J. Wu, and Z. Yang, "Intelligent fault diagnosis of rotating machinery via wavelet transform, generative adversarial nets and convolutional neural network," *Measurement*, vol. 159, Jul. 2020, Art. no. 107768.
[16] C. Heil, "Convolution and the Fourier transform," *Introduction Real Anal.*, vol. 280, pp. 327–3876, Jul. 2019.
[17] N. Huang, H. Chen, S. Zhang, G. Cai, W. Li, D. Xu, and L. Fang, "Mechanical fault diagnosis of high voltage circuit breakers based on wavelet time-frequency entropy and one-class support vector machine," *Entropy*, vol. 18, no. 1, p. 7, Dec. 2015.
[18] Y. Xing, M. Liu, P. Yang, Q. Peng, and B. Li, "Fault diagnosis method of HV circuit breaker based on wavelet packet time-frequency entropy and BP neural network," in *Proc. 29th Chin. Control Decis. Conf. (CCDC)*, May 2017, pp. 4200–4205.

[19] Z. Shutao, Z. Pei, S. Lu, and G. Jing, "Vibration and acoustic joint mechanical fault diagnosis method of high voltage circuit breakers," *Trans. China Electrotech. Soc.*, vol. 29, no. 7, pp. 216–221, 2014.
[20] J. Huang, X. Hu, and X. Geng, "An intelligent fault diagnosis method of high voltage circuit breaker based on improved EMD energy entropy and multi-class support vector machine," *Electr. Power Syst. Res.*, vol. 81, no. 2, pp. 400–407, Feb. 2011.
[21] Y. H. Sun, J. W. Wu, S. J. Lian, and L. M. Zhang, "Extraction of vibration signal feature vector of circuit breaker based on empirical mode decomposition amount of energy," *Trans. Chin. Electrotech. Soc.*, vol. 29, no. 3, pp. 228–236, Mar. 2014.
[22] M. Liu, B. Li, J. Zhang, and K. Wang, "An application of ensemble empirical mode decomposition and correlation dimension for the HV circuit breaker diagnosis," *Automatika*, vol. 60, no. 1, pp. 105–112, Jan. 2019.
[23] L. Mingliang, W. Keqi, S. Laijun, and Z. Jianju, "Applying empirical mode decomposition (EMD) and entropy to diagnose circuit breaker faults," *Optik*, vol. 126, no. 20, pp. 2338–2342, Oct. 2015.
[24] X. Zhang and J. Zhou, "Multi-fault diagnosis for rolling element bearings based on ensemble empirical mode decomposition and optimized support vector machines," *Mech. Syst. Signal Process.*, vol. 41, nos. 1–2, pp. 127–140, Dec. 2013.
[25] G. L. Li, M. X. Ming, X. Z. Gao, K. Miao, X. J. Ren, W. Y. Qi, and J. P. Zhu, "Fault diagnosis method of circuit breaker based on LMD and time spectrogram fractal dimension," *Instrum. Anal. Monitor.*, no. 4, pp. 1–5, Nov. 2018.
[26] N. Huang, H. Chen, G. Cai, L. Fang, and Y. Wang, "Mechanical fault diagnosis of high voltage circuit breakers based on variational mode decomposition and multi-layer classifier," *Sensors*, vol. 16, no. 11, p. 1887, Nov. 2016.
[27] L. Lin, Y. Wang, and H. Zhou, "Iterative filtering as an alternative algorithm for empirical mode decomposition," *Adv. Adapt. Data Anal.*, vol. 1, no. 4, pp. 543–560, Oct. 2009.
[28] K. Dragomiretskiy and D. Zosso, "Variational mode decomposition," *IEEE Trans. Signal Process.*, vol. 62, no. 3, pp. 531–544, Feb. 2014.
[29] Z. Lv, B. Tang, Y. Zhou, and C. Zhou, "A novel method for mechanical fault diagnosis based on variational mode decomposition and multikernel support vector machine," *Shock Vib.*, vol. 2016, pp. 1–11, Jan. 2016.
[30] L. Dou, S. Wan, and C. Zhan, "Application of multiscale entropy in mechanical fault diagnosis of high voltage circuit breaker," *Entropy*, vol. 20, no. 5, p. 325, Apr. 2018.
[31] X. Bi, J. Lin, D. Tang, F. Bi, X. Li, X. Yang, T. Ma, and P. Shen, "VMD-KFCM algorithm for the fault diagnosis of diesel engine vibration signals," *Energies*, vol. 13, no. 1, p. 228, Jan. 2020.
[32] C. Cao, M. Liu, and B. Li, "Mechanical fault diagnosis of high voltage circuit breakers utilizing VMD and optimal SVM classifier," in *Proc. Chin. Control Conf.*, Jul. 2019, pp. 4836–4841.
[33] S. Zhao and E. Wang, "Fault diagnosis of circuit breaker energy storage mechanism based on current-vibration entropy weight characteristic and grey wolf optimization–support vector machine," *IEEE Access*, vol. 7, pp. 86798–86809, 2019.
[34] S. Chen and X. Zhang, "Research of mechanical fault diagnosis method of circuit breaker based on VMD energy entropy and support vector machine," *Heilongjiang Electr. Power*, vol. 41, no. 1, pp. 60–63, Feb. 2019.
[35] B. Li, M. Liu, Z. Guo, and Y. Ji, "Mechanical fault diagnosis of high voltage circuit breakers utilizing EWT-improved time frequency entropy and optimal GRNN classifier," *Entropy*, vol. 20, no. 6, p. 448, Jun. 2018.
[36] Y. K. Zhang, X. Wang, and S. T. Wan, "Fault diagnosis of high-voltage circuit breaker based on VMD and fuzzy entropy," *Electr. Power Sci. Eng.*, vol. 35, no. 4, pp. 25–31, Apr. 2019.
[37] N. Huang, L. Fang, G. Cai, D. Xu, H. Chen, and Y. Nie, "Mechanical fault diagnosis of high voltage circuit breakers with unknown fault type using hybrid classifier based on LMD and time segmentation energy entropy," *Entropy*, vol. 18, no. 9, p. 322, Sep. 2016.
[38] L. J. Sun, X. G. Hu, and Y. C. Ji, "Fault diagnosis for high voltage circuit breakers with improved characteristic entropy of wavelet packet," *Proc. CSEE*, vol. 27, pp. 103–108, Dec. 2007.
[39] L. J. Sun, X. G. Hu, and Y. C. Ji, "Fault diagnosis for HV circuit breakers with characteristic entropy of wavelet packet," *Automat. Electron Power Syst.*, vol. 30, no. 14, pp. 62–65, Jul. 2006.
[40] T. Han, C. Liu, W. Yang, and D. Jiang, "Deep transfer network with joint distribution adaptation: A new intelligent fault diagnosis framework for industry application," *ISA Trans.*, vol. 97, pp. 269–281, Feb. 2020.
[41] S. Haidong, C. Junsheng, J. Hongkai, Y. Yu, and W. Zhantao, "Enhanced deep gated recurrent unit and complex wavelet packet energy moment entropy for early fault prognosis of bearing," *Knowl.-Based Syst.*, vol. 188, Jan. 2020, Art. no. 105022.
[42] T. Han, C. Liu, W. Yang, and D. Jiang, "A novel adversarial learning framework in deep convolutional neural network for intelligent diagnosis of mechanical faults," *Knowl.-Based Syst.*, vol. 165, pp. 474–487, Feb. 2019.
[43] Z. He, H. Shao, X. Zhang, J. Cheng, and Y. Yang, "Improved deep transfer auto-encoder for fault diagnosis of gearbox under variable working conditions with small training samples," *IEEE Access*, vol. 7, pp. 115368–115377, 2019.
[44] D. F. Specht, "Probabilistic neural networks," *Neural Netw.*, vol. 3, no. 1, pp. 109–118, Jan. 1990.
[45] L. X. Yang and Y. L. Zhu, "High voltage circuit breaker fault diagnosis of probabilistic neural network," *Power Syst. Protection Control*, vol. 43, no. 10, pp. 62–67, May 2015.
[46] Y. Yao and N. Wang, "Fault diagnosis model of adaptive miniature circuit breaker based on fractal theory and probabilistic neural network," *Mech. Syst. Signal Process.*, vol. 142, Aug. 2020, Art. no. 106772.
[47] Y. He, "Vibration signal acquisition system of engine based on LabVIEW," *Manuf. Automat.*, vol. 32, no. 9, pp. 196–198, Sep. 2010.
[48] L. G. Liu, J. H. Li, and L. H. Deng, "Design of data acquisition system based on LabVIEW," *Adv. Mater. Res.*, vol. 569, pp. 808–813, Sep. 2012.
[49] C. L. Liu, Y. J. Wu, and C. G. Zhen, "Rolling bearing fault diagnosis based on variational mode decomposition and fuzzy C means clustering," *Proc. CSEE*, vol. 35, no. 13, pp. 358–3365, May 2015.
[50] X. Jiao, B. Jing, Y. Huang, J. Li, and G. Xu, "Research on fault diagnosis of airborne fuel pump based on EMD and probabilistic neural networks," *Microelectron. Rel.*, vol. 75, pp. 808–813, Aug. 2017.

CHENGCHENG CAO was born in Shandong, China, in 1994. She is currently pursuing the master's degree in control science and engineering with Heilongjiang University. Her main research interests are intelligent detection, fault diagnosis, and signal processing.

MINGLIANG LIU was born in Heilongjiang, China, in 1980. He received the Ph.D. degree in forestry engineering automation from Northeast Forestry University, in 2017. He is currently a Full Professor and a Master's tutor with the School of Electrical Engineering, Heilongjiang University. His research interests include intelligent detection, fault diagnosis, signal processing, and pattern recognition.

BING LI was born in Hubei, China, in 1991. He received the master's degree in control science and engineering from Heilongjiang University in 2019. His main research interests are intelligent detection, fault diagnosis, and signal processing.

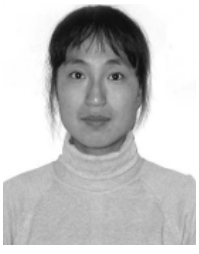

YUNXIA WANG was born in Shandong, China, in 1978. She received the M.S. degree in signal and information processing from Heilongjiang University, in 2008. She is currently working with the College of Electronic Engineering, Heilongjiang University. Her research interests include intelligent detection, fault diagnosis, and signal processing.